GSA Data Repository 2017104

Supplementary information: Stratigraphic unmixing reveals repeated hypoxia events over the past 500 years in the northern Adriatic Sea

Adam Tomašových, Ivo Gallmetzer, Alexandra Haselmair, Darrell S. Kaufman, Jelena Vidovic, Martin Zuschin

DETAILS ON METHODS

Sampling. Two closely spaced 1.5 m-long cores (M28 and M29) with a diameter of 16 cm were collected in 2013 in muddy sediments at 11 m water depth in Panzano Bay (45.7354ºN, 13.6005ºE). The total abundance of dead shells of *C. gibba* is 1029 individuals in the core M28 and 824 individuals in the core M29. The total abundance of living *C. gibba* individuals in grab samples penetrating through the uppermost 15 cm in 2014 is 1269 per m^2, out of 1441 molluscan individuals per m^2 in total (88% of the molluscan community). The cores were split into 2 cm-thick increments in the upper 20 cm and 5 cm-thick intervals in the lower part. Mollusks were sieved with a 1-mm mesh size and foraminifers were sieved with a 0.063-mm mesh size. All mollusk shells found were counted and identified to species level. In bivalves, the number of individuals of a given species corresponds to the number of single shells divided by two, plus the number of articulated valves. The sediment samples were split so that ~300 foraminifers were counted to determine species proportional abundances (Vidovic et al. 2016). The assignments of benthic foraminifers in the northern Adriatic to a hypoxia-sensitive group (*Ammonia beccarii*, genera *Buccella, Rosalina, Lenticulina*, and *Reussela* and species of the suborder Miliolina) follow Jannink (2001) and the assignments to a hypoxia-tolerant group (*Bulimina and Uvigerina*) follow Van der Zwaan and Jorissen (1991).

^{210}Pb analysis. The analysis was performed at the Low-Level Counting Labor Arsenal at the University of Natural Resources and Life Sciences in Vienna (Table DR1). Activities of ^{210}Pb and ^{226}Ra were analyzed in 2 cm-thick intervals in the upper 20 cm and in 5 cm-thick intervals between 20 and 40 cm by gamma spectrometry using a High Purity Germanium detector system. We compute apparent sediment-accumulation rates from the slope of the decay in excess ^{210}Pb according to the Constant Flux–Constant

Sedimentation model (CFCS, Sanchez-Cabeza and Ruiz-Fernandez 2012), avoiding the surface mixed layer (SML) that is defined here as the sediment depth over which excess ^{210}Pb levels remain constant (i.e., upper 6 cm).

Table DR1 ^{210}Pb sediment data (with standard deviations) measured in the uppermost 40 cm, with estimates of age.

Core	Depth midpoint (cm)	Total ^{210}Pb (Bq/kg)	^{226}Ra (Bq/kg)	^{210}Pb excess interpretation	210Pb age (before 2013 AD)	AAR median shell age (before 2013)
Panzano	0-2	126±7.56	25.7±1.8	mixed layer	4.2	17.6
Panzano	2-4	125±7.5	23.6±1.65	mixed layer	12.5	9.9
Panzano	4-6	127±7.62	25.8±2.06	mixed layer	20.9	NA
Panzano	6-8	109±7.63	24.4±1.95	decline in ^{210}Pb excess	29.2	39.6
Panzano	8-10	89±6.23	25.1±2.01	decline in ^{210}Pb excess	37.6	NA
Panzano	10-12	67±4.69	25.9±2.07	decline in ^{210}Pb excess	45.9	53.6
Panzano	12-14	75±5.25	26.8±2.14	decline in ^{210}Pb excess	54.3	NA
Panzano	14-16	51±4.08	24.9±1.99	decline in ^{210}Pb excess	62.6	NA
Panzano	16-18	49±3.92	26.2±2.1	decline in ^{210}Pb excess	71	64.35
Panzano	18-20	39±3.51	23.9±1.91	decline in ^{210}Pb excess	79.3	NA
Panzano	20-25	29±3.48	26.4±2.11	decline in ^{210}Pb excess	93.9	NA
Panzano	25-30	28±2.8	23.6±1.89	decline in ^{210}Pb excess	114.8	NA
Panzano	30-35	25±3.25	24.4±2.2	background	135.7	149
Panzano	35-40	27±3.24	23.7±1.9	background	NA	NA

Radiocarbon analyses. Eleven shells were selected for accelerator mass spectrometry (AMS) ^{14}C dating at the Poznan Radiocarbon Laboratory (Goslar et al. 2004), including five shells sampled offshore from Piran on the southern margin of the Gulf of Trieste at 24 m water depth. To avoid contamination, 30% of the outer shell mass was removed prior to AMS analysis in an ultrasonic bath and in 0.5M HCl, and then treated in 15% H_2O_2 for 10 min, again in an ultrasonic bath. The remaining carbonate was dissolved with concentrated H_3PO_4 in a vacuum line. Conventional ^{14}C ages were converted to calendar years (Table DR2) using Calib7.1 (Stuiver and Reimer 1993), the Marine13 data (Reimer et al. 2013), and a regional marine reservoir correction (ΔR) for the northeastern Adriatic (Rovinj) equal to = -61 years (standard deviation = 50 years)

(Siani et al. 2000). AAR-calibrated calendar ages are set relative to the year of the collection (2013 AD = year zero).

Table DR2 Radiocarbon ages of *Corbula gibba* collected in the Gulf of Trieste (Bay of Panzano and Piran) and used to calibrate the rate of amino acid racemization with D/L values of aspartic (Asp D/L) and glutamic acids (Glu D/L). Specimen IDs correspond to unique specimen identification numbers, Poznan IDs are the unique identification numbers used for radiocarbon analyses at the Poznan Radiocarbon Laboratory. Calibrated age (yrs) is relative to 2013 AD (the year of sampling).

Specimen ID	Poznan ID	Conventional 14C age	Conventional 14C age error (2 s.d.)	Calibrated age (median probability) BC/AD	Lower 95% conf. bound on calibrated age BC/AD	Upper 95% conf. bound on calibrated age BC/AD	Calibrated age (to 2013 AD)	Lower 95% conf. bound on calibrated age	Upper 95% conf. bound on calibrated age	Asp D/L	Glu D/L
Pan M28 30-35 6	Poz-71958	515	58	1750	1630	1910	263	383	103	0.12	0.038
Pan M28 110-115 15	Poz-71961	610	58	1626	1494	1729	387	519	284	0.151	0.033
Pan M28 110-115 19	Poz-71962	1140	78	1197	1040	1321	816	973	692	0.168	0.036
Pan M28 125-130 1	Poz-71963	660	58	1584	1476	1684	429	537	329	0.138	0.031
Pan M28 125-130 18	Poz-71964	615	58	1620	1488	1726	393	525	287	0.156	0.028
Pan 128 145-150 01	Poz-71965	1000	58	1324	1229	1424	689	784	589	0.191	0.05
PiranII M53 85-90 01	Poz-78510	8010	71	-6581	-6782	-6425	8594	8795	8438	0.372	0.136
PiranII M53 85-90 02	Poz-78511	7970	78	-6541	-6740	-6385	8554	8753	8398	0.447	0.155
PiranII M53 100-105 02	Poz-78512	8120	71	-6737	-6991	-6553	8750	9004	8566	0.41	0.149
PiranII M53 100-105 03	Poz-78513	8010	71	-6581	-6782	-6425	8594	8795	8438	0.393	0.131
PiranII M53 65-70 10	Poz-78515	5250	64	-3726	-3904	-3615	5739	5917	5628	0.335	0.143
Panzano grab7-2							1	2	0.1	0.039	0.019
Panzano grab7-3							1	2	0.1	0.041	0.02
Panzano grab7-7							1	2	0.1	0.038	0.018

Amino-acid racemization (AAR). AAR was analyzed on 328 specimens of *C. gibba* selected from 12 increments in the core M28, with midpoints at 1 (0-2 cm), 3 (2-4 cm), 7 (6-8 cm), 11 (10-12 cm), 17 (16-18 cm), 32.5 (30-35 cm), 47.5 (45-50 cm), 62.5

(60-65 cm, plus few shells sampled at 67.5 cm), 92.5 (90-95 cm, plus few shells sampled at 87.5 cm), 112.5 (110-115 cm), 127.5 (125-130 cm), and 147.5 cm (145-150 cm). Thirty specimens were selected at random from each increment, or all specimens were used if the interval contained fewer than 30. For analyses of raw stratigraphic changes in abundance of *C. gibba* in both cores, the pairs of adjacent 2-cm increments in the upper 20 cm were pooled into 4-cm segments. AAR analysis was carried out at Northern Arizona University using reverse-phase high-pressure liquid chromatography (RP-HPLC) and the procedures of Kaufman and Manley (1998). Specimens were cleaned by removing 20% by weight with a dilute solution of HCl, then dissolved in 7 M HCl. The resulting solutions were hydrolysed at 110°C for 6 hours to release amino acids from the peptide chains to recover the total hydrolysable amino acid population (Kaufman and Manley 1998). Eighteen specimens were flagged as outliers according to screening criteria outlined by Kosnik and Kaufman (2008), and the 311 dead shells were thus used for dating, analyses of sedimentation rate, mixing, and history of *C. gibba* production. After this screening, the numbers of specimens in increments are as follows: 23 shells in 0-2 cm, 28 shells in 2-4 cm, 29 shells in 6-8 cm, 27 shells in 10-12 cm, 27 shells in 16-18 cm, 26 shells in 30-35 cm, 28 shells in 45-50 cm, 26 shells in 60-65 cm (plus 3 shells sampled at 67.5 cm), 16 shells in 90-95 (plus 12 shells sampled at 87.5 cm), 29 shells in 110-115 cm, 25 shells in 125-130 cm, and 12 shells in 145-150 cm.

AMS-AAR calibration. Asp and Glu D/L values of 14 shells were fit using four mathematical functions to model the relation between age and D/L values, with two uncertainty models (lognormal and gamma), with the initial D/L value fixed to zero or estimated from age data (Allen et al. 2013). The model with the smallest Bayesian information criterion (BIC) is the time-dependent reaction kinetic model for Asp, with the initial D/L value estimated from data (TDK1), and lognormal uncertainty (Fig. DR1, Table DR3). The final shell age corresponds to median age based on the Bayesian posterior distributions of age estimates predicted by TDK1 model.

Table DR3 Calibration statistics for the rate of amino acid racemization (AAR) based on paired AAR and radiometric analyses of *Corbula gibba* and two models of uncertainty,

showing models with Bayes Information Criterion (BIC) values less than 6 units relative to the model with minimum BIC. Explanations: APK = apparent parabolic kinetics; CPK = constrained power-law kinetics; SPK = simple power-law kinetics; TDK = time-dependent reaction kinetics; 0 = the initial D/L value is fixed at zero; 1 = the initial D/L value is estimated from data, *a-d* -model parameters, R0 - the D/L value at time 0.

Model	Amino acid	mu.func	ln(a)	ln(b)	c	R0	ln(d)	BIC	ΔBIC
Gamma uncertainty									
SPK0	Asp	gamma	11.431	0.972	NA	0.000	4.784	191.21	0.00
TDK0	Asp	gamma	11.100	0.895	NA	0.000	5.029	192.36	1.15
SPK1	Asp	gamma	11.414	0.973	-69.299	0.000	4.822	193.86	2.65
TDK1	Asp	gamma	11.119	0.906	-45.744	0.000	4.958	194.96	3.75
APK0	Glu	gamma	12.873	NA	NA	0.000	5.837	196.97	5.76
Lognormal uncertainty									
TDK1	Asp	lognormal	11.408	0.937	0.606	0.028	-2.896	172.95	0.00

Sedimentation rates. The chronology based on the CFCS model and apparent sedimentation rates based on ^{210}Pb equal to 0.24 cm/year imply that the upper 30 cm accumulated during the last century. The uppermost 6 cm show uniform activities of excess ^{210}Pb and thus determine the surface mixed layer, followed by a relatively monotonic decline down to 30 cm, and by the appearance of background values at 30-40 cm (Table DR1, Fig. 2a). Stratigraphic changes in median shell age of *C. gibba* are not linear and show a slower decline in age between 30 cm and 150 cm (from 1615 to 1864, i.e., 0.48 cm/year) than above 30 cm (from 1864 to 2014, i.e., 0.2 cm/year).

Time averaging. We estimate *raw* time averaging of individual increments with inter-quartile age range (IQAR). Age uncertainty associated with calibrating the rate of AAR (analytical measurement errors and by intra-specimen variability in D/L) tends to increase with age (Fig. DR1). Such error structure generates an apparent increase in age range of older assemblages. To estimate the degree of this bias, we estimate the magnitude of this error and its contribution to the raw IQAR in individual increments, applying the approach of Dominguez et al. (2016). The distribution of age estimates predicted by the TDK1 model with lognormal uncertainty, expected purely due to the calibration error, can be used to estimate an IQAR for each shell. The mean IQAR of all shells in a given increment represent the error component. The *corrected* time averaging refers then to the difference between raw IQAR and this error component.

Surface age-frequency distributions. Fitting the AFD from the upper 6 cm to the one-phase exponential function (assuming constant loss rate of shells from the mixed layer) results in a loss rate of $\lambda = 0.035$, i.e., the mean time to shell loss from the SML (either via disintegration or burial) is 29 years. The goodness of fit of two more complex models (see Tomašových et al. 2014) where loss rate can change in time is not better than in the one-phase exponential model (AICc [one-phase exponential] = 446.82, AICc [Weibull] = 446.74, AICc [two-phase exponential] = 447.02). If λ fully corresponds to burial, then burial rate below the mixed layer occurs at ~0.2 cm/year. This estimate, based on the steepness of the AFD, approximately matches the sedimentation rate estimated from down-core changes in ^{210}Pb (0.24 cm/year). Therefore, although disintegration probably contributes to the loss rate λ, its contribution is minor because time to burial according to other approaches is similar.

Reconstructing past production. Abundance of shells observed in individual increments is a function of their mixing, disintegration, and burial. We reconstruct past production of *C. gibba* in three steps. In the first two steps, we account for mixing. In the third step, we discuss our approach that accounts for loss of shells via disintegration and burial. In the absence of variable production or under simple changes in production that follow unimodal or rectangular trajectories, loss of shells can be directly estimated from age-frequency data, with models that allow for age-dependent changes in disintegration or burial (Weibull or two-phase exponential models, Tomašových et al. 2014, 2016). This approach becomes less straightforward under more complex changes in production.

First, we approximate the shape of AFDs of undated increments by (1) pooling distributions of dated increments below and above the undated increment into a single distribution, and (2) estimating mean and standard deviation of such pooled distribution. AFDs in individual increments are normal-shaped below the surface mixed layer and separation between median ages between directly-dated increments is smaller than time averaging of these increments, thus allowing us to approximate their shape with a normal distribution (using normal distribution truncated on the lower interval equal to zero in R package msm, Jackson 2016). This pooling approach should be conservative in terms of detecting major fluctuations in original production.

Second, we resample shells to the total number of *C. gibba* in each increment, either sampling shells from increment-specific age-frequency distributions (AFDs), or from interpolated normal distributions, and count the number of resampled shells in individual 10-year cohorts. The number of resampled *C. gibba* shells in each increment is based on the sum of the shells in both cores. The total number of shell ages reconstructed by this approach is thus the sum of all shells in both cores (i.e., 1,853 shells). The resulting distribution of shell ages in all increments represents the AFD of *all* shells in the core.

Third, we assume that disintegration rates in the surface mixed layer are minor relative to shell burial rates because the fit of surface AFD to the exponential model implies that loss rates of shells from the surface mixed layer primarily correspond to sedimentation rates as estimated by ^{210}Pb data (Fig. 1, Fig. DR2) or to shell burial rates as estimated by the stratigraphic decline in median shell age in the upper 30 cm of the core. Therefore, we primarily account for loss of shells via burial below the 1.5 m and neglect shell loss by disintegration. We divide the whole-core AFD (as reconstructed in the first two steps above) by the survival function (where survival refers to shells that were not lost from the core) of the exponential model (Tomašových et al. 2016). Fitting the whole-core AFD with the exponential model leads to $\lambda = 0.0052$, but this value is probably an overestimate due to stronger production since 1800s. Median shell date increases between 30 cm and 150 cm from 1615 to 1864 (i.e., shell burial rate is 0.48 cm/years), and above 30 cm from 1864 to 2014 (0.2 cm/years). Therefore, the net whole-core burial rate of shells is ~0.424 cm/year, implying that mean time to burial of shells below 1.5 m can be expected to be ~354 years ($\lambda = 0.0028$).

This approach allows us to unmix the original signatures of ecological history from the raw stratigraphic record. Repeating such re-sampling and interpolation 1,000 times and pooling ages into 10-year cohorts generates a mean abundance per age cohort (Table DR4) with 95% confidence intervals. These reconstructions are compared with stratigraphic trends in both the absolute and proportional abundance of *C. gibba* directly observed in sediment cores but obscured by bioturbation. Given that *C. gibba* lives for ~5 years (Jones 1956), the reconstructed abundances of individuals in 10 year cohorts per

184 0.04 m^2 can be extrapolated to standing density/m^2 by a factor of 12.5 (rather than by a
185 factor of 25).
186
187 **Table DR4** Absolute and proportional abundances of *C. gibba* in cores M28 and M29
188 and reconstructed abundances (10 year cohorts per 0.04 m^2) that account for mixing and
189 burial effects. Median ages of *C. gibba* in undated increments are based on linear
190 interpolation of median ages in increments located stratigraphically below and above.
191

	Sediment depth (cm)	Median *C. gibba* age	M28 abundance	M29 abundance	M28 proportion	M29 proportion	Reconstructed (unmixed) abundance	Reconstructed (unmixed) abundance (with burial)
M28 - 2	2	1998	37	46	0.25	0.38	56.1	58.2
M28 - 6	6	1973	70	47	0.42	0.34	85.7	95.0
M28 - 10	10	1959	61	39	0.44	0.38	78.4	90.4
M28 - 14	14	1954	54	80	0.27	0.39	67.6	78.9
M28 - 18	18	1949	35	44	0.24	0.22	58.0	68.8
M28 - 22.5	22.5	1920.7	25	34	0.13	0.20	43.5	55.8
M28 - 27.5	27.5	1892.3	48	38	0.19	0.21	63.0	87.6
M28 - 32.5	32.5	1864	38	36	0.19	0.30	56.7	85.5
M28 - 37.5	37.5	1853	60	36	0.29	0.24	49.0	75.9
M28 - 42.5	42.5	1842	115	24	0.42	0.20	39.0	62.4
M28 - 47.5	47.5	1831	44	27	0.28	0.18	38.3	63.2
M28 - 52.5	52.5	1823.7	30	20	0.23	0.19	40.0	67.3
M28 - 57.5	57.5	1816.3	21	13	0.18	0.20	47.9	82.7
M28 - 62.5	62.5	1809	23	20	0.22	0.27	57.6	101.0
M28 - 67.5	67.5	1805	28	12	0.32	0.32	55.0	97.5
M28 - 72.5	72.5	1801	17	10	0.19	0.22	52.3	93.9
M28 - 77.5	77.5	1797	18	14	0.23	0.36	48.6	88.1
M28 - 82.5	82.5	1793	8	3	0.13	0.09	44.4	81.5
M28 - 87.5	87.5	1789	9	12	0.10	0.14	42.2	78.4
M28 - 92.5	92.5	1785	17	9	0.15	0.14	45.7	85.8
M28 - 97.5	97.5	1768.5	17	22	0.17	0.26	33.1	65.3
M28 - 102.5	102.5	1752	25	41	0.23	0.33	32.5	66.8
M28 - 107.5	107.5	1735.5	26	22	0.28	0.21	27.6	59.4
M28 - 112.5	112.5	1719	30	19	0.32	0.32	24.3	54.9
M28 - 117.5	117.5	1714	28	19	0.39	0.34	22.6	51.7
M28 - 122.5	122.5	1709	22	23	0.29	0.32	21.0	48.8
M28 - 127.5	127.5	1704	27	21	0.36	0.44	20.2	47.5
M28 - 132.5	132.5	1681.75	43	33	0.36	0.42	16.4	40.8

M28 - 137.5	137.5	1659.5	26	24	0.21	0.27	10.5	27.8
M28 - 142.5	142.5	1637.25	13	13	0.19	0.20	18.2	51.8
M28 - 147.5	147.5	1615	14	23	0.21	0.24	13.8	41.9

Relations between C. gibba and environment. Frequency distributions of temperature and water depths with occurrences of *Corbula gibba* in the Mediterranean Sea obtained from the OBIS database (Ocean Biogeographic Information 2016, Fig. DR3) shows that the median temperature inhabited by *C. gibba* is 18ºC and that the median water depth is 22 m. *C. gibba* in the Northeastern Atlantic ranges to highermost latitudes and is also extremely frequent between 50-60ºN. Therefore, this species primarily inhabits cool- and warm-temperate habitats. The present-day mean annual sea-surface temperature in Panzano Bay is ~17 ºC, with monthly minima and maxima equal to 8.2 ºC and 26.2 ºC. Given that the frequency of *C. gibba* occurrences in the Mediterranean Sea markedly declines above 19ºC, populations of *C. gibba* in northernmost Adriatic are rather near the upper edge of their temperature tolerance, and an increase in seawater temperature would unlikely contribute to their outbreaks.

We determined cross-correlation between five environmental variables on one hand (mean annual temperature, and mean seasonal precipitation for four seasons) and abundance of *C. gibba* on the other hand, using data spanning from 1600 to 2000 (the earliest abundances from the 16th century with small values are probably affected by a large sampling noise). First, we determined the environmental residuals from the first-order autoregressive model (AR1). Second, *C. gibba* abundance were filtered by the coefficients of the AR1 model determined for a given environmental variable. Third, we estimated cross-correlation between the environmental residuals and filtered abundance values. Sea-surface temperatures up to 1979 are based on alkenones (produced by haptophyte algae) from on the Gulf of Taranto (Versteegh et al. 2007; Taricco et al. 2009), supplemented by instrumental annual sea surface temperatures (SST) extracted for Gulf of Taranto from Hadley Centre Sea Ice and Sea Surface Temperature (HadISST1.1) data (Rayner et al. 2003) (at 44.5°N and 13.5°E). Precipitation data are based on Pauling et al. (2006) at 13.75ºE and 45.75ºN (Gulf of Trieste). Temperature data of Versteegh et al. (2007) were upscaled to 10-year averages. Yearly precipitation data were scaled up

with 10-year moving window average in order to compare them with abundances of *C. gibba* in 10-year cohorts.

Raw Pearson cross-correlation between SST and *C. gibba* abundance, not accounting for autocorrelation, is $r = 0.72$ ($p < 0.0001$). Raw Pearson cross-correlation between SST and *C. gibba* abundance, not accounting for autocorrelation, is $r = 0.72$ ($p < 0.0001$). Pearson cross-correlation between SST and *C. gibba* abundance (Fig. DR4) at the second lag is equal to 0.31 ($p < 0.05$) (Fig. DR4). Pearson cross-correlation between winter North Atlantic Oscillation index (Luterbacher et al. 2002) and *C. gibba* abundance is also positive ($r = 0.3$, $p < 0.05$) (Fig. DR4). Cross-correlations between precipitation data and *C. gibba* abundance are weak and insignificant (Fig. DR4).

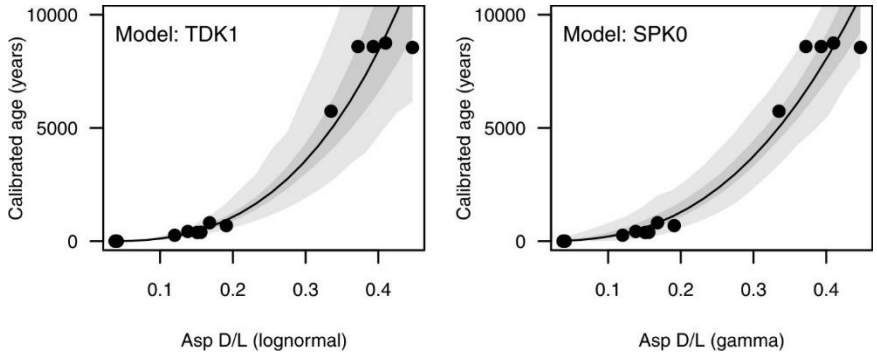

Figure DR1 Amino acid racemization calibrated by radiocarbon ages based on 14 shells of *C. gibba*. Relation between postmortem age (determined by ^{14}C) and D/L values of aspartic acid for *Corbula gibba*, best-fit by TDK1(time-dependent reaction kinetics) and SPK0 (simple power-law kinetics with the initial D/L value fixed at zero) models, respectively, on the basis of BIC, and assuming log-normal and gamma distributions for the residuals, including data from live-collected specimens as calibration data points. Light grey envelopes correspond to 95% prediction intervals for the age of a given specimen; dark grey envelopes correspond to 95% confidence intervals for median age. Five shells with the oldest ages were collected in a sediment core sampled in the Bay of Piran.

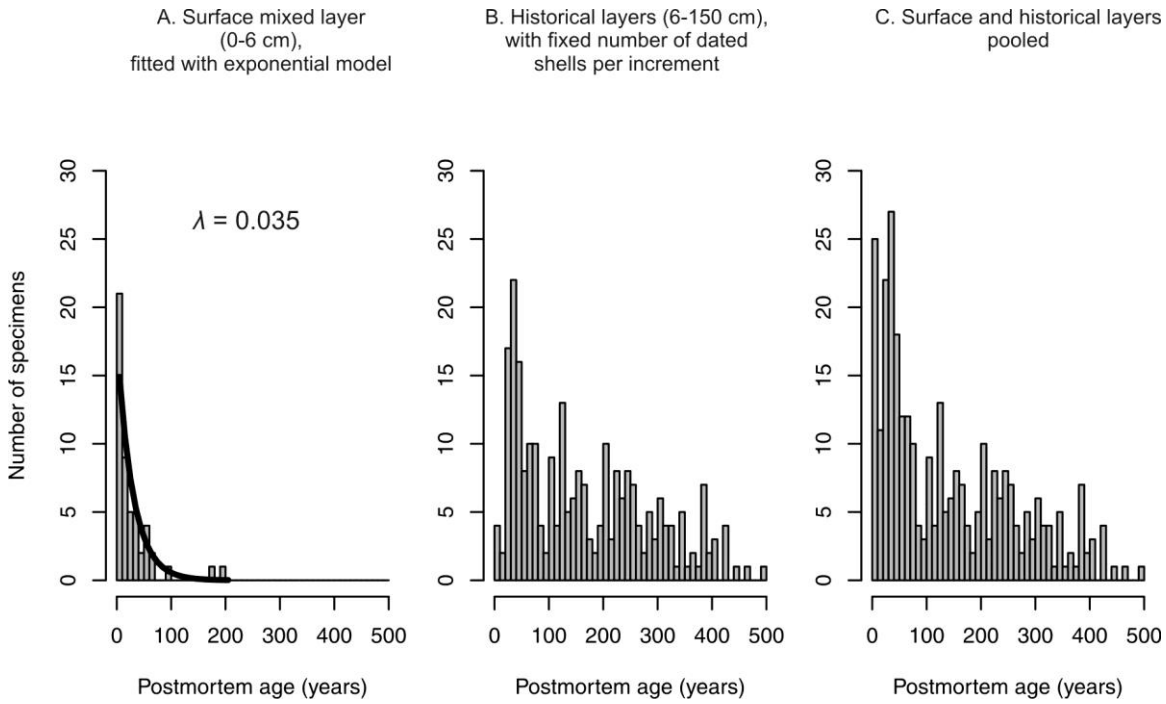

Figure DR2 Empirical surface (A) and subsurface (B) age-frequency distributions (AFDs) of *C. gibba*, and (C) age-frequency distribution generated by pooling all increments. The black solid line represents the fit of the one-phase exponential distribution. Rate of shell loss estimated by the exponential model from the surface mixed layer is congruent with the sedimentation rate based on ^{210}Pb. Subsurface AFD shows signs of multimodality but is based on the fixed (~30) number of shells per increment.

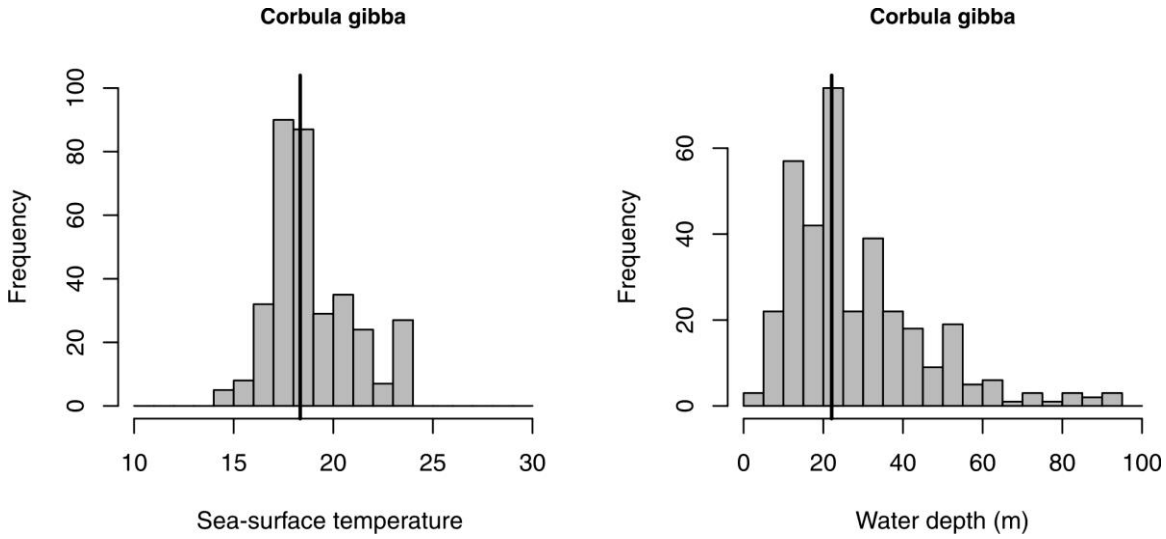

Figure DR3 – Frequency distribution of temperature and water depths with occurrences of *Corbula gibba.* The median temperature is 18ºC, and the frequency of occurrences markedly declines at 19ºC. The median water depth is 22 m. The present-day mean annual sea-surface temperature in Panzano Bay is ~17 ºC, with monthly minima and maxima equal to 8.2 ºC and 26.2 ºC.

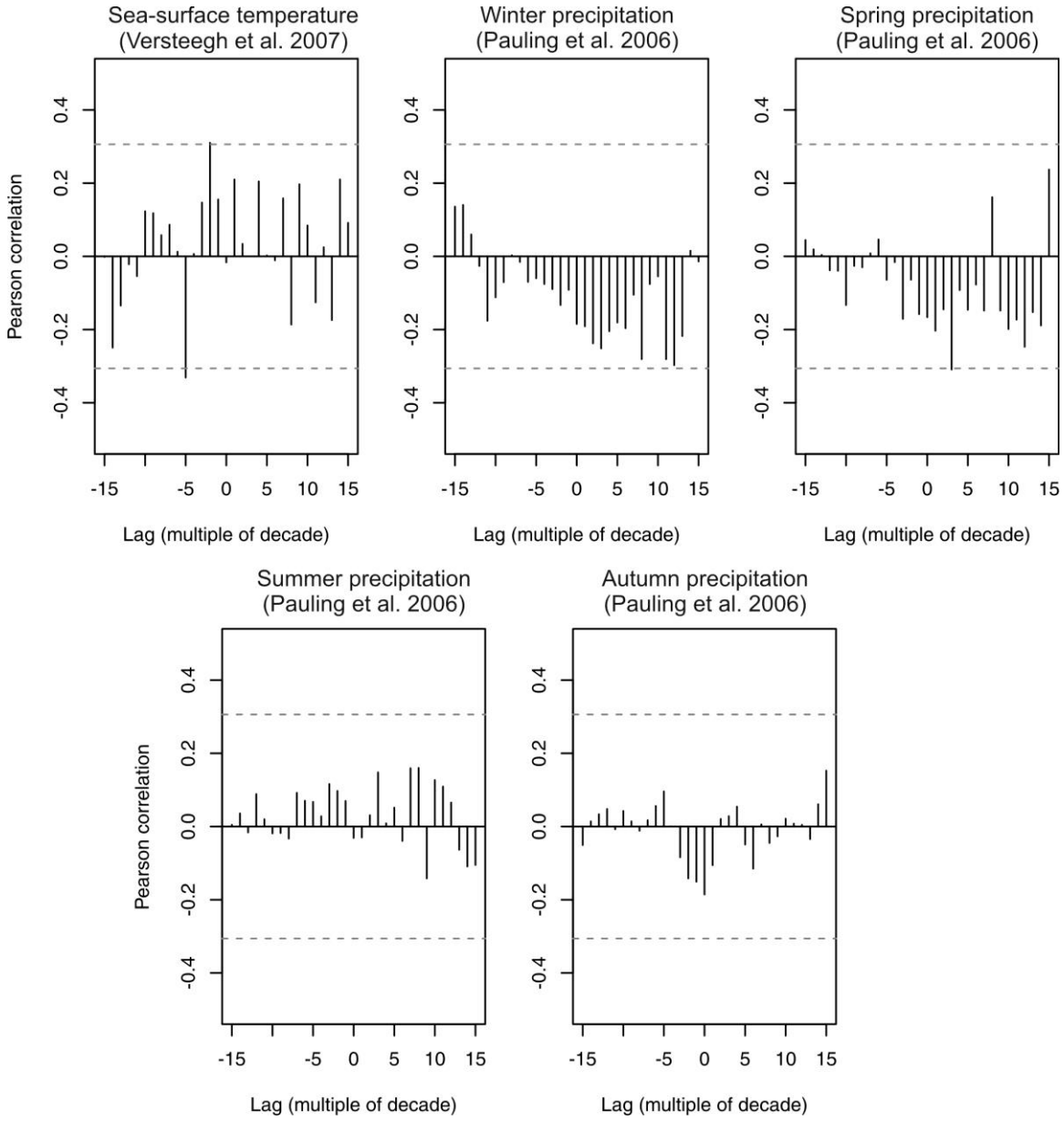

Figure DR4 Cross-correlations between the residuals of five environmental variables fitted to a first-order autoregressive model (AR1) and abundance of *C. gibba* (reconstructed on the basis of unmixing and incorporating burial effects) filtered by AR1 model. Dashed lines correspond to a significance level of 0.05.

References

Allen AP, Kosnik MA, Kaufman DS (2013) Characterizing the dynamics of amino acid racemization using time-dependent reaction kinetics: a Bayesian approach to fitting age-calibration models. Quaternary Geochronology, **18**, 63-77.

Dominguez JG, Kosnik MA, Allen AP, Hua Q, Jacob DE, Kaufman DS, Whitacre KE (2013) Time-averaging and stratigraphic resolution in death assemblages and Holocene deposits: Sydney Habour's molluscan record. Palaios, **31**, 564-575.

Goslar T, Czernik J, Goslar E (2004) Low-energy ^{14}C AMS in Poznań Radiocarbon Laboratory, Poland. Nuclear Instruments and Methods B, **223-224**, 5-11.

Jackson C (2016) msm: Multi-state Markov and hidden Markov models in continuous time. R package version 1.6.1. https://cran.r-project.org/web/packages/msm/index.html

Jannink NT, Van der Zwaan GJ, Almogi-Labin A, Duijnstee I, Jorissen FJ (2001) A transfer function for the quantitative reconstruction of oxygen contents in marine paleoenvironments. Geologica Ultraiectina, **203**, 161–169.

Jones NS, Slinn, DJ (1956) The fauna and biomass of a muddy sand deposit off Port Erin, Isle of Man: with an appendix on methods used for the analysis of deposits. Journal of Animal Ecology, **25**, 217-252.

Kaufman DS, Manley WF (1998) A new procedure for determining DL amino acid ratios in fossils using reverse phase liquid chromatography. Quaternary Science Reviews, **17**, 987–1000.

Kosnik MA, Kaufman DS (2008) Identifying outliers and assessing the accuracy of amino acid racemization measurements for geochronology: II. Data screening. Quaternary Geochronology, **3**, 328-341.

Luterbacher J, Xoplaki E, Dietrich D, Jones PD, Davies TD, Portis D, Gonzalez-Rouco JF, Von Storch H, Gyalistras D, Casty C, Wanner H (2001) Extending North Atlantic oscillation reconstructions back to 1500. Atmospheric Science Letters, **2**, 114-124.

Ocean Biogeographic Information System (2016) Intergovernmental Oceanographic Commission of UNESCO. www.iobis.org. Accessed: 2016-11-30.

Pauling, A, Luterbacher J, Casty C, Wanner H (2006) Five hundred years of gridded high-resolution precipitation reconstructions over Europe and the connection to large-scale circulation. Climate Dynamics, **26**, 387-405.

Rayner NA, Parker DE, Horton EB, Folland CK, Alexander LV, Rowell DP, Kent EC, Kaplan A (2003) Global analyses of sea surface temperature, sea ice, and night marine air temperature since the late nineteenth century. Journal of Geophysical Research, **108**, No. D14, 4407 10.1029/2002JD002670

Reimer P, Bard E, Bayliss A, Beck JW, Blackwell PG, Bronk R *et al* (2013) IntCal13 and Marine13 radiocarbon age calibration curves 0–50,000 years cal BP. Radiocarbon, **55**, 1869-1887.

Sanchez-Cabeza JA, Ruiz-Fernández AC (2012) ^{210}Pb sediment radiochronology: an integrated formulation and classification of dating models. Geochimica et Cosmochimica Acta, **82**, 183-200.

Siani G, Paterne M, Arnold M, Bard E, Métivier B, Tisnerat N, Bassinot F (2000) Radiocarbon reservoir ages in the Mediterranean Sea and Black Sea. Radiocarbon, **42**, 271-280.

Stuiver M, Reimer PJ (1993) Extended ^{14}C data base and revised CALIB 3.0 C age calibration program. Radiocarbon, **35**, 215–230.

Taricco C, Ghil M, Alessio S, Vivaldo G (2009) Two millennia of climate variability in the Central Mediterranean. Climate of the Past, **5**, 171-181.

Tomašových A, Kidwell SM, Foygel Barber R, Kaufman DS (2014) Long-term accumulation of carbonate shells reflects a 100-fold drop in loss rate. Geology, **42**, 9, 819-822.

Tomašových A, Kidwell, SM, Foygel Barber R (2016) Inferring skeletal production from time-averaged assemblages: skeletal loss pulls the timing of production pulses towards the modern period. Paleobiology **42**, 54-76.

Van der Zwaan GJ, Jorissen FJ (1991) Biofacial patterns in river-induced shelf anoxia. Geological Society, London, Special Publications, **58**, 65-82.

Vidovic J, Nawrot R, Gallmetzer I, Haselmair A, Tomasovych A, Stachowitsch M, Cosovic V, Zuschin M (2016) Anthropogenically induced environmental changes in the northeastern Adriatic Sea in the last 500 years (Panzano Bay, Gulf of Trieste). Biogeosciences, **13**, 5965-5981.

Versteegh GJM, De Leeuw JW, Taricco C, Romero A (2007) Temperature and productivity influences on U37K′ and their possible relation to solar forcing of the

331 Mediterranean winter. Geochemistry, Geophysics, Geosystems, **8**, Q09005.

Table DR3 Amino acid racemization data for 311 specimens of *Corbula gibba*, and estimated calendar age based on radiocarbon calibration. The second column refers to the bottom boundary of an increment in which each specimen was found (2 cm-thick increments in the upper 20 cm, and 4 cm-thick increments below), the third column refers to the bottom boundary of pooled increments (i.e., pairs of 2 cm-thick increments in the top 20 cm pooled to 4 cm-thick increments) as analyzed in Figure 1A.

Specimen ID	Max. increment depth (cm)	Max. increment depth (pooled 4-5 cm increments)	Postmortem age (y)	Asp D/L	Glu D/L
Pan M28-0-2-001	2	4	64	0.087	0.026
Pan M28-0-2-002	2	4	10	0.057	0.023
Pan M28-0-2-003	2	4	8	0.055	0.023
Pan M28-0-2-004	2	4	7	0.053	0.022
Pan M28-0-2-005	2	4	37	0.076	0.031
Pan M28-0-2-006	2	4	30	0.072	0.029
Pan M28-0-2-007	2	4	53	0.083	0.027
Pan M28-0-2-008	2	4	7	0.053	0.024
Pan M28-0-2-009	2	4	15	0.062	0.026
Pan M28-0-2-010	2	4	37	0.076	0.027
Pan M28-0-2-011	2	4	1	0.04	0.02
Pan M28-0-2-013	2	4	58	0.085	0.026
Pan M28-0-2-014	2	4	33	0.074	0.026
Pan M28-0-2-015	2	4	12	0.059	0.025
Pan M28-0-2-016	2	4	22	0.067	0.028
Pan M28-0-2-017	2	4	8	0.055	0.024
Pan M28-0-2-018	2	4	18	0.064	0.029
Pan M28-0-2-019	2	4	26	0.07	0.028
Pan M28-0-2-020	2	4	13	0.06	0.027
Pan M28-0-2-021	2	4	16	0.063	0.024
Pan M28-0-2-022	2	4	11	0.058	0.027
Pan M28-0-2-023	2	4	176	0.115	0.036
Pan M28-0-2-024	2	4	198	0.119	0.03
Pan M28-10-12-001	12	12	56	0.084	0.032
Pan M28-10-12-002	12	12	61	0.086	0.029

Pan M28-10-12-003	12	12	70	0.089	0.029
Pan M28-10-12-004	12	12	39	0.077	0.029
Pan M28-10-12-006	12	12	73	0.09	0.029
Pan M28-10-12-007	12	12	46	0.08	0.028
Pan M28-10-12-008	12	12	112	0.101	0.03
Pan M28-10-12-009	12	12	209	0.121	0.033
Pan M28-10-12-010	12	12	35	0.075	0.024
Pan M28-10-12-011	12	12	37	0.076	0.025
Pan M28-10-12-012	12	12	28	0.071	0.027
Pan M28-10-12-013	12	12	44	0.079	0.026
Pan M28-10-12-014	12	12	22	0.067	0.026
Pan M28-10-12-015	12	12	64	0.087	0.026
Pan M28-10-12-016	12	12	30	0.072	0.024
Pan M28-10-12-017	12	12	53	0.083	0.028
Pan M28-10-12-018	12	12	48	0.081	0.024
Pan M28-10-12-019	12	12	53	0.083	0.029
Pan M28-10-12-020	12	12	48	0.081	0.026
Pan M28-10-12-022	12	12	33	0.074	0.029
Pan M28-10-12-023	12	12	89	0.095	0.03
Pan M28-10-12-024	12	12	266	0.13	0.039
Pan M28-10-12-026	12	12	61	0.086	0.036
Pan M28-10-12-027	12	12	26	0.07	0.02
Pan M28-10-12-028	12	12	70	0.089	0.032
Pan M28-10-12-029	12	12	35	0.075	0.028
Pan M28-10-12-030	12	12	266	0.13	0.039
Pan M28-110-115-001	115	115	388	0.146	0.032
Pan M28-110-115-002	115	115	294	0.134	0.033
Pan M28-110-115-003	115	115	203	0.12	0.033
Pan M28-110-115-004	115	115	5	0.051	0.026
Pan M28-110-115-005	115	115	308	0.136	0.035
Pan M28-110-115-006	115	115	227	0.124	0.036
Pan M28-110-115-007	115	115	240	0.126	0.034
Pan M28-110-115-008	115	115	301	0.135	0.031
Pan M28-110-115-009	115	115	323	0.138	0.045
Pan M28-110-115-010	115	115	347	0.141	0.041
Pan M28-110-115-011	115	115	316	0.137	0.033
Pan M28-110-115-012	115	115	120	0.103	0.033
Pan M28-110-115-013	115	115	380	0.145	0.039
Pan M28-110-115-014	115	115	273	0.131	0.031
Pan M28-110-115-015	115	115	387	0.151	0.033
Pan M28-110-115-016	115	115	339	0.14	0.033
Pan M28-110-115-017	115	115	294	0.134	0.029
Pan M28-110-115-018	115	115	246	0.127	0.029

Pan M28-110-115-019	115	115	816	0.168	0.036
Pan M28-110-115-020	115	115	156	0.111	0.043
Pan M28-110-115-021	115	115	323	0.138	0.04
Pan M28-110-115-022	115	115	209	0.121	0.028
Pan M28-110-115-023	115	115	116	0.102	0.029
Pan M28-110-115-024	115	115	227	0.124	0.032
Pan M28-110-115-025	115	115	142	0.108	0.034
Pan M28-110-115-026	115	115	301	0.135	0.039
Pan M28-110-115-027	115	115	308	0.136	0.031
Pan M28-110-115-028	115	115	128	0.105	0.028
Pan M28-110-115-029	115	115	96	0.097	0.028
Pan M28-125-130-001	130	130	429	0.138	0.031
Pan M28-125-130-002	130	130	388	0.146	0.032
Pan M28-125-130-003	130	130	233	0.125	0.035
Pan M28-125-130-004	130	130	380	0.145	0.032
Pan M28-125-130-005	130	130	108	0.1	0.03
Pan M28-125-130-006	130	130	128	0.105	0.03
Pan M28-125-130-007	130	130	142	0.108	0.031
Pan M28-125-130-008	130	130	347	0.141	0.031
Pan M28-125-130-009	130	130	259	0.129	0.034
Pan M28-125-130-010	130	130	171	0.114	0.032
Pan M28-125-130-011	130	130	156	0.111	0.032
Pan M28-125-130-012	130	130	128	0.105	0.03
Pan M28-125-130-013	130	130	405	0.148	0.049
Pan M28-125-130-014	130	130	423	0.15	0.034
Pan M28-125-130-015	130	130	423	0.15	0.036
Pan M28-125-130-016	130	130	371	0.144	0.041
Pan M28-125-130-017	130	130	363	0.143	0.034
Pan M28-125-130-018	130	130	393	0.156	0.028
Pan M28-125-130-019	130	130	308	0.136	0.034
Pan M28-125-130-020	130	130	423	0.15	0.031
Pan M28-125-130-021	130	130	100	0.098	0.028
Pan M28-125-130-022	130	130	137	0.107	0.029
Pan M28-125-130-023	130	130	405	0.148	0.031
Pan M28-125-130-024	130	130	246	0.127	0.037
Pan M28-125-130-025	130	130	287	0.133	0.03
Pan M28-145-150-001	150	150	689	0.191	0.05
Pan M28-145-150-002	150	150	509	0.159	0.032
Pan M28-145-150-003	150	150	166	0.113	0.032
Pan M28-145-150-004	150	150	166	0.113	0.033
Pan M28-145-150-005	150	150	1628	0.232	0.048
Pan M28-145-150-006	150	150	489	0.157	0.044
Pan M28-145-150-007	150	150	509	0.159	0.046

Pan M28-145-150-008	150	150	405	0.148	0.039
Pan M28-145-150-011	150	150	388	0.146	0.04
Pan M28-145-150-014	150	150	316	0.137	0.034
Pan M28-145-150-015	150	150	161	0.112	0.033
Pan M28-145-150-016	150	150	142	0.108	0.032
Pan M28-16-18-001	18	20	70	0.089	0.031
Pan M28-16-18-002	18	20	100	0.098	0.028
Pan M28-16-18-003	18	20	46	0.08	0.026
Pan M28-16-18-004	18	20	83	0.093	0.026
Pan M28-16-18-005	18	20	287	0.133	0.034
Pan M28-16-18-006	18	20	83	0.093	0.026
Pan M28-16-18-007	18	20	93	0.096	0.023
Pan M28-16-18-008	18	20	56	0.084	0.025
Pan M28-16-18-009	18	20	39	0.077	0.026
Pan M28-16-18-011	18	20	79	0.092	0.03
Pan M28-16-18-012	18	20	64	0.087	0.027
Pan M28-16-18-013	18	20	37	0.076	0.027
Pan M28-16-18-014	18	20	64	0.087	0.023
Pan M28-16-18-015	18	20	79	0.092	0.03
Pan M28-16-18-016	18	20	215	0.122	0.033
Pan M28-16-18-017	18	20	61	0.086	0.026
Pan M28-16-18-018	18	20	37	0.076	0.021
Pan M28-16-18-019	18	20	151	0.11	0.038
Pan M28-16-18-020	18	20	116	0.102	0.031
Pan M28-16-18-021	18	20	48	0.081	0.024
Pan M28-16-18-022	18	20	146	0.109	0.044
Pan M28-16-18-023	18	20	42	0.078	0.027
Pan M28-16-18-024	18	20	26	0.07	0.022
Pan M28-16-18-026	18	20	22	0.067	0.027
Pan M28-16-18-027	18	20	28	0.071	0.024
Pan M28-16-18-028	18	20	61	0.086	0.02
Pan M28-16-18-029	18	20	70	0.089	0.028
Pan M28-2-4-001	4	4	44	0.079	0.022
Pan M28-2-4-002	4	4	93	0.096	0.029
Pan M28-2-4-003	4	4	39	0.077	0.023
Pan M28-2-4-004	4	4	46	0.08	0.028
Pan M28-2-4-005	4	4	61	0.086	0.025
Pan M28-2-4-006	4	4	7	0.053	0.022
Pan M28-2-4-007	4	4	9	0.056	0.024
Pan M28-2-4-008	4	4	16	0.063	0.024
Pan M28-2-4-009	4	4	7	0.054	0.023
Pan M28-2-4-010	4	4	5	0.051	0.022
Pan M28-2-4-011	4	4	8	0.055	0.022

Pan M28-2-4-012	4	4	11	0.058	0.022
Pan M28-2-4-013	4	4	4	0.049	0.02
Pan M28-2-4-014	4	4	10	0.057	0.022
Pan M28-2-4-016	4	4	10	0.057	0.024
Pan M28-2-4-017	4	4	15	0.062	0.024
Pan M28-2-4-018	4	4	51	0.082	0.027
Pan M28-2-4-019	4	4	1	0.041	0.02
Pan M28-2-4-020	4	4	58	0.085	0.032
Pan M28-2-4-021	4	4	4	0.049	0.025
Pan M28-2-4-022	4	4	5	0.051	0.024
Pan M28-2-4-023	4	4	5	0.051	0.021
Pan M28-2-4-024	4	4	5	0.051	0.024
Pan M28-2-4-025	4	4	5	0.051	0.023
Pan M28-2-4-026	4	4	31	0.073	0.029
Pan M28-2-4-027	4	4	25	0.069	0.028
Pan M28-2-4-029	4	4	28	0.071	0.029
Pan M28-2-4-030	4	4	4	0.048	0.024
Pan M28-30-35-001	35	35	287	0.133	0.038
Pan M28-30-35-002	35	35	31	0.073	0.028
Pan M28-30-35-004	35	35	137	0.107	0.037
Pan M28-30-35-006	35	35	263	0.12	0.038
Pan M28-30-35-007	35	35	161	0.112	0.029
Pan M28-30-35-008	35	35	266	0.13	0.035
Pan M28-30-35-009	35	35	19	0.065	0.023
Pan M28-30-35-010	35	35	259	0.129	0.034
Pan M28-30-35-011	35	35	20	0.066	0.025
Pan M28-30-35-012	35	35	58	0.085	0.026
Pan M28-30-35-013	35	35	26	0.07	0.025
Pan M28-30-35-015	35	35	137	0.107	0.029
Pan M28-30-35-016	35	35	46	0.08	0.028
Pan M28-30-35-018	35	35	44	0.079	0.03
Pan M28-30-35-019	35	35	240	0.126	0.035
Pan M28-30-35-020	35	35	156	0.111	0.034
Pan M28-30-35-021	35	35	37	0.076	0.025
Pan M28-30-35-022	35	35	203	0.12	0.03
Pan M28-30-35-023	35	35	240	0.126	0.035
Pan M28-30-35-024	35	35	233	0.125	0.033
Pan M28-30-35-025	35	35	198	0.119	0.026
Pan M28-30-35-026	35	35	142	0.108	0.029
Pan M28-30-35-027	35	35	203	0.12	0.038
Pan M28-30-35-028	35	35	108	0.1	0.026
Pan M28-30-35-029	35	35	156	0.111	0.033
Pan M28-30-35-030	35	35	51	0.082	0.032

Pan M28-45-50-001	50	50	280	0.132	0.034
Pan M28-45-50-002	50	50	252	0.128	0.03
Pan M28-45-50-003	50	50	233	0.125	0.035
Pan M28-45-50-004	50	50	120	0.103	0.029
Pan M28-45-50-005	50	50	192	0.118	0.027
Pan M28-45-50-007	50	50	209	0.121	0.03
Pan M28-45-50-008	50	50	20	0.066	0.022
Pan M28-45-50-009	50	50	120	0.103	0.039
Pan M28-45-50-010	50	50	18	0.064	0.023
Pan M28-45-50-011	50	50	70	0.089	0.028
Pan M28-45-50-012	50	50	233	0.125	0.025
Pan M28-45-50-013	50	50	380	0.145	0.04
Pan M28-45-50-014	50	50	171	0.114	0.028
Pan M28-45-50-015	50	50	259	0.129	0.034
Pan M28-45-50-016	50	50	28	0.071	0.022
Pan M28-45-50-017	50	50	252	0.128	0.031
Pan M28-45-50-018	50	50	108	0.1	0.029
Pan M28-45-50-019	50	50	37	0.076	0.023
Pan M28-45-50-025	50	50	146	0.109	0.033
Pan M28-45-50-031	50	50	31	0.073	0.024
Pan M28-45-50-032	50	50	192	0.118	0.029
Pan M28-45-50-033	50	50	252	0.128	0.03
Pan M28-45-50-034	50	50	124	0.104	0.029
Pan M28-45-50-035	50	50	280	0.132	0.031
Pan M28-45-50-036	50	50	397	0.147	0.028
Pan M28-45-50-037	50	50	316	0.137	0.032
Pan M28-45-50-038	50	50	156	0.111	0.031
Pan M28-45-50-039	50	50	31	0.073	0.023
Pan M28-60-65-01	65	65	171	0.114	0.03
Pan M28-60-65-02	65	65	161	0.112	0.024
Pan M28-60-65-03	65	65	203	0.12	0.029
Pan M28-60-65-04	65	65	221	0.123	0.031
Pan M28-60-65-05	65	65	89	0.095	0.024
Pan M28-60-65-06	65	65	181	0.116	0.025
Pan M28-60-65-07	65	65	227	0.124	0.035
Pan M28-60-65-08	65	65	192	0.118	0.029
Pan M28-60-65-09	65	65	323	0.138	0.03
Pan M28-60-65-10	65	65	331	0.139	0.036
Pan M28-60-65-11	65	65	112	0.101	0.027
Pan M28-60-65-12	65	65	215	0.122	0.032
Pan M28-60-65-13	65	65	323	0.138	0.031
Pan M28-60-65-14	65	65	156	0.111	0.034
Pan M28-60-65-15	65	65	203	0.12	0.028

Pan M28-60-65-16	65	65	273	0.131	0.026
Pan M28-60-65-17	65	65	294	0.134	0.034
Pan M28-60-65-18	65	65	203	0.12	0.026
Pan M28-60-65-19	65	65	355	0.142	0.032
Pan M28-60-65-20	65	65	133	0.106	0.027
Pan M28-60-65-21	65	65	104	0.099	0.028
Pan M28-60-65-22	65	65	108	0.1	0.026
Pan M28-60-65-23	65	65	70	0.089	0.028
Pan M28-60-65-24	65	65	227	0.124	0.03
Pan M28-60-65-25	65	65	161	0.112	0.027
Pan M28-60-65-26	65	65	42	0.078	0.023
Pan M28-65-70-022	70	65	221	0.123	0.033
Pan M28-65-70-023	70	65	124	0.104	0.027
Pan M28-65-70-030	70	65	209	0.121	0.026
Pan M28-6-8 01	8	8	39	0.077	0.034
Pan M28-6-8 02	8	8	70	0.089	0.029
Pan M28-6-8 03	8	8	39	0.077	0.027
Pan M28-6-8 04	8	8	33	0.074	0.023
Pan M28-6-8 05	8	8	28	0.071	0.02
Pan M28-6-8 06	8	8	67	0.088	0.024
Pan M28-6-8 07	8	8	37	0.076	0.021
Pan M28-6-8 08	8	8	22	0.067	0.024
Pan M28-6-8 09	8	8	31	0.073	0.022
Pan M28-6-8 10	8	8	46	0.08	0.027
Pan M28-6-8 11	8	8	46	0.08	0.025
Pan M28-6-8 12	8	8	28	0.071	0.023
Pan M28-6-8 13	8	8	100	0.098	0.034
Pan M28-6-8 14	8	8	20	0.066	0.026
Pan M28-6-8 15	8	8	28	0.071	0.023
Pan M28-6-8 16	8	8	44	0.079	0.025
Pan M28-6-8 17	8	8	53	0.083	0.028
Pan M28-6-8 18	8	8	35	0.075	0.026
Pan M28-6-8 19	8	8	61	0.086	0.028
Pan M28-6-8 20	8	8	53	0.083	0.024
Pan M28-6-8 21	8	8	48	0.081	0.023
Pan M28-6-8 22	8	8	37	0.076	0.026
Pan M28-6-8 23	8	8	20	0.066	0.022
Pan M28-6-8 24	8	8	8	0.055	0.021
Pan M28-6-8 25	8	8	35	0.075	0.022
Pan M28-6-8 26	8	8	46	0.08	0.024
Pan M28-6-8 28	8	8	37	0.076	0.028
Pan M28-6-8 29	8	8	46	0.08	0.034
Pan M28-6-8 30	8	8	61	0.086	0.031

Pan M28-85-90-001	90	95	233	0.125	0.032
Pan M28-85-90-003	90	95	363	0.143	0.035
Pan M28-85-90-004	90	95	246	0.127	0.033
Pan M28-85-90-005	90	95	215	0.122	0.032
Pan M28-85-90-006	90	95	128	0.105	0.026
Pan M28-85-90-007	90	95	4	0.049	0.027
Pan M28-85-90-008	90	95	124	0.104	0.03
Pan M28-85-90-009	90	95	166	0.113	0.026
Pan M28-85-90-010	90	95	259	0.129	0.033
Pan M28-85-90-012	90	95	104	0.099	0.037
Pan M28-85-90-013	90	95	124	0.104	0.027
Pan M28-85-90-014	90	95	227	0.124	0.029
Pan M28-90-95-001	95	95	461	0.154	0.033
Pan M28-90-95-002	95	95	8	0.055	0.023
Pan M28-90-95-003	95	95	128	0.105	0.03
Pan M28-90-95-004	95	95	181	0.116	0.029
Pan M28-90-95-005	95	95	137	0.107	0.031
Pan M28-90-95-006	95	95	347	0.141	0.028
Pan M28-90-95-007	95	95	316	0.137	0.03
Pan M28-90-95-008	95	95	227	0.124	0.03
Pan M28-90-95-009	95	95	347	0.141	0.033
Pan M28-90-95-010	95	95	442	0.152	0.031
Pan M28-90-95-011	95	95	151	0.11	0.034
Pan M28-90-95-012	95	95	308	0.136	0.034
Pan M28-90-95-013	95	95	233	0.125	0.033
Pan M28-90-95-014	95	95	240	0.126	0.031
Pan M28-90-95-015	95	95	120	0.103	0.034
Pan M28-90-95-018	95	95	240	0.126	0.032

339